Journal of Physiology (1991), **441**, *pp.* 537–557
With 14 figures
Printed in Great Britain

CHANGES IN EXCITABILITY OF HUMAN MOTOR AXONS UNDERLYING POST-ISCHAEMIC FASCICULATIONS: EVIDENCE FOR TWO STABLE STATES

BY H. BOSTOCK, M. BAKER AND G. REID

From the Sobell Department of Neurophysiology, Institute of Neurology, Queen Square, London WC1N 3BG

(*Received 4 February 1991*)

SUMMARY

1. We have investigated the origin of post-ischaemic ectopic discharges in human nerve by recording changes in electrical excitability following periods of ischaemia (15–20 min) sufficient to induce spontaneous motor fasciculations. The ulnar nerve was stimulated beneath a pressure cuff on the upper arm, and compound motor action potentials recorded from abductor digiti minimi.

2. On releasing the cuff after 15 min of ischaemia, thresholds to short current pulses increased in two distinct phases: a slow phase followed by a rapid rise to a peak threshold. The rapid rise was too fast to track (i.e. 100% threshold increase in less than 4 s), and was sometimes followed after 30–40 s by an equally rapid fall. Small polarizing currents affected the timing of the rapid threshold increase, as if it was occurring at a particular membrane potential.

3. By recording complete stimulus–response curves every few seconds, we found that the rapid threshold changes were associated with a bimodal distribution of thresholds. Most fibres were found in either a high-threshold or low-threshold state, and these two states converged over a period of about 10 min.

4. Spontaneous motor fasciculations were only recorded after the rapid rise in threshold and when the fibres existed in two threshold states. The spontaneous activity was not responsible for inducing the two states, since they could also be recorded in its absence.

5. A computer model of a human motor axon node and internode was constructed, incorporating channel types demonstrated in other axons, and channel densities adjusted to match the responses of human axons to depolarizing and hyperpolarizing current pulses. An increase in extracellular potassium concentration produced a region of negative slope conductance in the current–voltage relationship of the model, and the appearance of two stable states with enhanced activity of the electrogenic sodium pump.

6. Transitions between the two stable states of the model could account qualitatively for the rapid threshold changes recorded from post-ischaemic axons. In the model, spontaneous action potentials occurred following some transitions from the high potential state to the low potential state. We suggest that post-ischaemic motor fasciculations in man also involve transitions between two

equilibrium states, occurring in axons with high extracellular potassium and high electrogenic pump activity.

INTRODUCTION

This paper extends the observations of the preceding one (Bostock, Baker, Grafe & Reid, 1991), on post-ischaemic excitability changes in human motor axons, to longer periods of ischaemia that give rise to spontaneous motor fasciculations. This type of motor activity was studied by Kugelberg (1946) and Kugelberg & Cobb (1951). Kugelberg and Cobb used a proximal anaesthetic block and a distal pressure cuff to show that the discharges originated ectopically within the previously ischaemic limb, and not centrally or in the motor nerve terminals. Kugelberg (1946) also showed that the post-ischaemic axons discharged with a characteristic pattern of high frequency (100–180 Hz) bursts of impulses, repeated at intervals of as long as a second. This was very different from the ectopic firing pattern that could be induced during ischaemia. Kugelberg found that the most proximal parts of the longest motor axons, which were also the parts most susceptible to ischaemic conduction failure, were the most liable to generate ectopic impulses. In all of these respects, post-ischaemic motor fasciculations resemble the post-ischaemic paraesthesiae studied by Merrington & Nathan (1949) and the corresponding neural activity recorded by Ochoa & Torebjörk (1980). The motor fasciculations only occur after longer durations of ischaemia, however, and are relatively short lived.

In the preceding paper it was found that the changes in excitability and accommodation following ischaemia up to 10 min, though profound, were not such as to predict the occurrence of spontaneous discharges by simple extrapolation to longer periods. Hyperpolarization by the sodium pump, which seemed to be the main factor involved, would not on its own be expected to trigger action potentials. To understand the origin of the post-ischaemic discharges, we have therefore recorded at the site where excitability changes were found to be greatest, i.e. under the pressure cuff, under conditions found to induce discharges reliably in a few fibres. We found evidence for very rapid changes in excitability occurring without obvious cause, and evidence that the post-ischaemic axons could exist in two distinct states, a low-threshold and a high-threshold state.

These observations recalled a paper by Stämpfli (1959), describing experiments on isolated frog nodes exposed to high potassium concentrations. He found that the membrane potential did not always fall immediately, and proposed that axons could exist in two stable equilibrium states: a high membrane potential state with low potassium conductance (Condition 1), and a low membrane potential state with high potassium conductance (Condition 2). Hyperpolarizing currents helped to stabilize Condition 1 over Condition 2. To test whether Stämpfli's two state hypothesis could apply to post-ischaemic human motor axons, we have also modelled a human motor axon in high potassium and the effects of varying pump current. The mathematical model has provided a plausible explanation for the abrupt threshold changes observed. It has also led to a new hypothesis for the origin of the spontaneous action potentials.

METHODS

Recordings from human motor nerve

The experiments described in this paper all involved stimulating the ulnar nerve with short (1–2 ms) current pulses under a pressure cuff on the upper arm, and recording compound motor action potentials (CMAP) from abductor digiti minimi (ADM) with surface electrodes. The methods

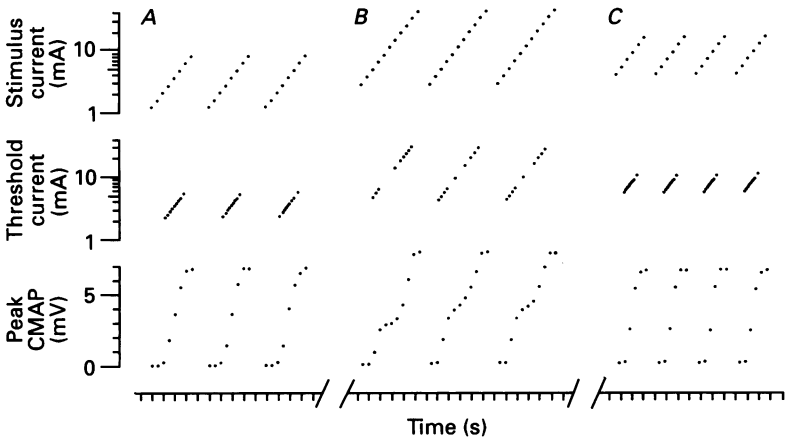

Fig. 1. Derivation of threshold distributions from stimulus response recordings. Top, sequence of stimulus current amplitudes delivered to ulnar nerve under pressure cuff (logarithmic scale). Bottom, peak amplitudes of the CMAPs recorded from ADM. Middle, derived thresholds, i.e. interpolated stimulus currents required to evoked CMAPs 10%, 20%,.... 90% of maximal (logarithmic scale). Stimulus–response behaviour illustrated *A* during ischaemia, *B*, during early post-ischaemic period when threshold distribution became bimodal, and *C* after recovery from ischaemia. The dots representing derived thresholds in the middle plot are reproduced on a linear scale in Fig. 7 at 5, 18 and 40 min.

were described in the preceding paper (Bostock *et al.* 1991). One additional protocol was used which is illustrated in Fig. 1. Stimulus–response curves were generated every few seconds, by increasing the stimulus current in 31·8% steps from a sub-minimal to a supra-maximal level (upper plot in Fig. 1). Steps were added or subtracted from either end as the experiment proceeded, to ensure that the full range of thresholds was encompassed, and the rapid post-ischaemic rise in threshold was anticipated by increasing the maximum stimulus strength to 40 mA. Peak amplitudes of the CMAPs were detected by an analogue circuit and sampled by the PDP11/23 computer (lower plot in Fig. 1). The maximal CMAP amplitude varied slightly during the experiment, declining by about 15% during the last 5 min of ischaemia, and with a modest post-ischaemic overshoot (Fig. 1*B*). The peak CMAPs were therefore first converted to percentages of the maximal CMAP in each complete stimulus–response sequence. Threshold distributions were then plotted in one of two ways. For Fig. 8*B* the percentage responses for the same stimulus were averaged over 15–30 s and the response to the next lower stimulus subtracted. The height of each column plotted corresponds to the percentage contribution to the CMAP recruited by a 31·8% stimulus increase. Alternatively, thresholds as a function of time were plotted as dots (Fig. 1 middle plot, Figs 7 and 8). The stimulus required to elicit a CMAP, 10% of maximal was estimated by linear interpolation between the stimuli that produced CMAPs next below, and next above 10%. This was represented by one dot at the appropriate time, and the process repeated for 20%, 30% etc. up to 90% of maximal CMAP. Each dot therefore represents a stimulus that recruits another 10% of the CMAP.

An electrical model of human motor axons

To model a node and internode of a human motor axon, we started with the equivalent circuit proposed for frog and lizard myelinated axons by Barrett & Barrett (1982), and found applicable

to rat spinal root fibres by Baker, Bostock, Grafe & Martius (1987). The membrane resistances were substituted with equivalent circuits for some of the types of ion channel demonstrated in rat myelinated axons (Fig. 2). In the earlier study (Baker *et al.* 1987) it was found that electrotonus in rat spinal roots treated with tetrodotoxin to block sodium channels could be explained by fast

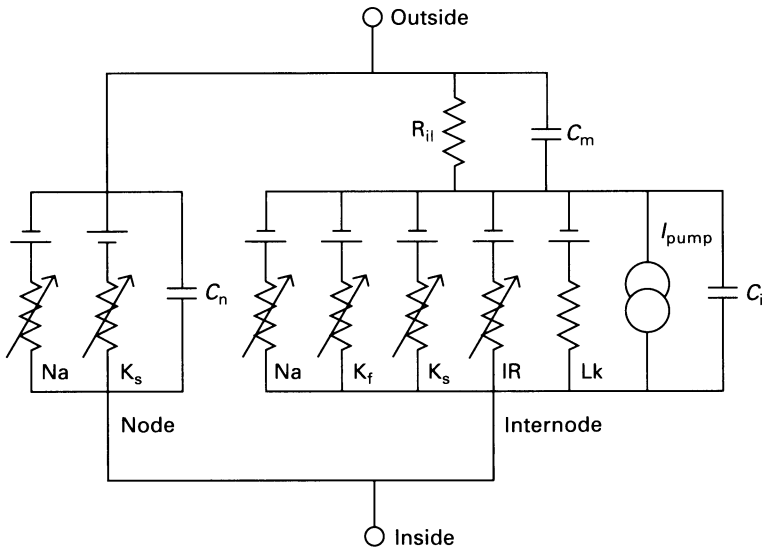

Fig. 2. Equivalent circuit used to model electrical behaviour of human motor axons. Model comprises single node and internode, equivalent to a space-clamped fibre, elaborated from Fig. 8*B* in Barrett & Barrett (1982). This diagram correctly shows the serial/parallel arrangement of current sources modelled, but the currents were calculated from permeabilities according to constant field theory, rather than from equilibrium potentials and conductances. C_n, nodal capacity (1·5 pF). C_i, capacity of internodal axon (350 pF). C_m, capacity of myelin sheath (2 pF). R_{il}, internodal leak resistance due to pathways through myelin sheath and axoglial junctions (50 MΩ). I_{pump}, net outward current generated by electrogenic Na^+–K^+ pump (0·1 nA). Channel types and maximum permeabilities ($cm^{-3} \times 10^9$): node, sodium (Na, 4), slow potassium (K_s, 0·18); internode, sodium (Na, 80), fast potassium (K_f, 7), slow potassium (K_s, 2), inward rectifier (IR, 0·01), leak (Lk, 0·0064).

(K_f) and slow (K_s) potassium channels at the nodes, and additionally inward rectifier (IR) channels in the internodes. On the basis of the work of Grissmer (1986), Chiu & Schwarz (1987) and Shrager (1989), sodium channels were included in the internodal axolemma, as well as at the nodes. A nodal K_f conductance has been omitted for simplicity, since it has generally been found small in mammalian fibres, and we found that threshold electrotonus in rat nerve became more similar to that in human motor axons after reducing the K_f conductance with 4-aminopyridine (Bostock & Baker, 1988).

To maintain ionic and electrical equilibrium in the resting state, the resting efflux of K^+ ions through potassium (K_f, K_s) and inward rectifier (IR) channels was assumed to be balanced by an influx of K^+ ions driven by the sodium pump. The outward Na^+ current driven by the pump (3/2 times the inward K^+ current) was only partially balanced by the resting inward current through the inward rectifier. To keep the resting sodium current in balance, we introduced a small, sodium specific leakage conductance (Lk). The net outward pump current (I_{pump}) was assumed to be generated in the internode, where most of the resting passive fluxes occurred (see Discussion).

Kinetics for sodium and K_f channels were taken from published data for rat nerves at 37 °C (Schwarz & Eikhof, 1987), except that the m, h parameters were shifted 4 mV in the hyperpolarizing direction. An 'ultra-slow' sodium inactivation parameter u, with a slope factor of −12 mV and a

value of 0·7 at resting potential (Fox, 1976) was included in the steady-state equations, but its kinetics were not modelled. K_s channels were assumed to follow symmetrical Boltzmann kinetics for a single gating particle, with 50% activation at −60 mV (Dubois, 1981; Roper & Schwarz, 1989). Evidence for inward rectification in rat internodes was presented by Baker *et al.* (1987), but it has not been characterized by voltage clamp. The axonal IR channels are activated by hyperpolarization, and appear to resemble those responsible for I_h in sensory ganglion neurones (Mayer & Westbrook, 1983) or I_Q in hippocampal pyramidal neurones (Halliwell & Adams, 1982), rather than those in muscle or glial membranes (Leech & Stanfield, 1981; Barres, Chun & Corey, 1988). Activation of the IR channels was assumed to be independent of E_K, with a half-activation potential of −110 mV: this is in the range of 20–25 mV negative to the resting potential found in sensory ganglion and hippocampal neurones (Mayer & Westbrook, 1983). The IR channels were modelled as permeable to Na^+ as well as K^+ ions, with an equilibrium potential close to 0 mV. Only the sodium channels were assumed to inactivate. To allow for the effects of altered ion concentrations, all channel currents were assumed to obey the constant field equation.

It was considered of primary importance that the accommodative properties of the model should closely match those of the human axons. On the basis that 'threshold electrotonus' can accurately reflect electrotonic changes in membrane potential (Baker & Bostock, 1989), the other parameters were adjusted to match electrotonus in the model with recordings of threshold electrotonus in H.B.'s ulnar nerve (see Fig. 9). A sensitive variable in this respect was the resting potential. The value of −86·7 mV (or −86 mV for the internodal membrane) was arrived at by trial and error. Two parameters were not critical for electrotonus, but helped determine the behaviour in high potassium: internodal Na^+ permeability was set at 20 times the nodal, a figure in line with the findings of Shrager (1989) and Chiu & Schwarz (1987) on rat nerve; the internodal K_f permeability was required to counter a large steady-state inward current due to the internodal Na^+ channels in depolarized axons. The data set used for the model at rest is listed below.

Parameters and equations of model. $R_{il} = 50\ M\Omega$, $C_i = 350$ pF, $C_m = 2$ pF, $C_n = 1{\cdot}5$ pF. Permeabilities ($cm^3\ s^{-1} \times 10^{-9}$): Na, 4; K_s, 0·18; Na*, 80; K_f*, 7; K_s*, 2; IR*, 0·01; Lk*, 0·0064; where * denotes internodal quantity. Resting state: $E_r = -86{\cdot}7$ mV, $E_r^* = -86$ mV, $I_{pump} = 0{\cdot}1$ nA, where E denotes absolute membrane potential. Passive ion fluxes: Na^+, 0·3 nA inwards; K^+, 0·2 nA outwards. Ion concentrations (mM): $[Na^+]_i$, 9; $[Na^+]_o$, 144·2; $[K^+]_i$, 155; $[K^+]_o$, 3. Nodal and internodal membrane potentials are given by the differential equations:

$$dE/dt = -(I_{Na} + I_{K_s} + I_{ex} - (E^* - E)/R_{il})/(C_n + C_m)$$

$$dE^*/dt = -(I_{Na}^* + I_{K_f}^* + I_{K_s}^* + I_{IR}^* + I_{LK}^* + I_{pump} + (E^* - E)/R_{il} - C_m\, dE/dt)/C_i,$$

where $I_{Na} = P_{Na}\, m^3 h u\, z(\mathrm{Na})$; $I_{K_f} = P_{K_f}\, n^2\, z(\mathrm{K})$; $I_{K_s} = P_{K_s}\, s\, z(\mathrm{K})$; $I_{IR} = P_{IR}\, q(0{\cdot}53 z(\mathrm{Na}) + 0{\cdot}47 z(\mathrm{K}))$; $I_{Lk} = P_{Lk}\, z(\mathrm{Na})$; I_{ex} = external current and $z(X) = EF^2/RT)\,([X]_o - [X]_i \exp(EF/RT))/(1 - \exp(EF/RT))$ for X = Na, K ($T = 310$ K). The fraction activations are given by the differential equation:

$$dx/dt = a_x(1-x) - b_x x \quad \text{for } x = m,h,n,s,q$$

where

	A (ms^{-1})	B (mV)	C (mV)
a_m	1·872	−56·59	6·06
b_m	3·973	−61	9·41
a_h	0·550	−109·74	9·06
b_h	22·61	−26	12·5
a_n	0·129	−53	10
b_n	0·324	−78	10
s	0·00556	−60	22
q	0·00125	−110	−12
u		−80	−12

and a_m, $a_n = A(E-B)/(1-\exp((B-E)/C))$; b_m, a_h, $b_n = A(B-E)/(1-\exp((E-B)/C))$; $b_h = A/(1+\exp((B-E)/C))$; a_s, $a_q = A\exp((E-B)/C)$; b_s, $b_q = A/(\exp((E-B)/C))$; $u = 0{\cdot}7/(1+\exp((B-E_r)/C))$.

The equations for a single node and internode, representing a spatially uniform axon, were integrated by Euler's method with Fortran on the PDP 11/23. The integration step corresponded to a minimum nodal potential step of 2 mV or a minimum time interval of 0·01 ms, whichever was

less; except that when there was no danger of impulse generation the minimum time interval was increased to 0·1 ms, and sodium activation and inactivation were assumed to be instantaneous.

RESULTS

Recordings from human motor nerve

At first we found that the occurrence of post-ischaemic motor fasciculations varied considerably between one subject and another, and between one ischaemic episode and another in the same nerve. We then found that a fairly consistent pattern of modest post-ischaemic fasciculations could be evoked in H.B.'s left ADM, with a cuff just above the elbow inflated for 5 min, and after an interval of 25 min for another 15 min. In eight repeats of this protocol, at intervals of at least 24 h, post-ischaemic discharges lasted for an average of 4·7 min (range 2·5–10). (The sensitivity of this phenomenon to the protocol is indicated by the observation that on two occasions when 15 min of ischaemia was not preceded by 5 min of ischaemia, or preceded by 5 min of ischaemia at a greater interval, no motor activity was recorded.) The excitability changes, tested with 1 or 2 ms current pulses, were only consistent as well if we tracked the stimuli required to evoke a CMAP of a particular size. For the example illustrated in Fig. 3, we tracked a $\frac{1}{5}$ maximal CMAP.

Compared with the threshold recordings for shorter durations of ischaemia described in the preceding paper, there was a conspicuous 'notch', which corresponded closely in time with the spontaneous motor activity. To test whether the activity could be causing the notch (e.g. by the test pulse occurring while fibres were superexcitable after spontaneous impulses) the subject later produced a comparable motor discharge by voluntary activation. This had no discernible effect on the recorded threshold, and the same was true in another experiment when the voluntary activity immediately followed the spontaneous discharge. This evidence was not conclusive, since the units recorded voluntarily may have had relatively high thresholds for electrical stimulation. In another experiment, however, (when the 15 min of ischaemia was not preceded by 5 min of ischaemia) we recorded a 'notch' without any motor fasciculations.

The threshold 'notch' illustrated in Fig. 3 was best seen when we tracked a CMAP in the range $\frac{1}{4}$ to $\frac{1}{8}$ maximal. To compare directly the excitability changes in fibres of different excitability, we switched the recording gain repeatedly to track the thresholds of $\frac{1}{2}$, $\frac{1}{4}$, $\frac{1}{8}$ and $\frac{1}{40}$ maximal CMAPs. At the highest gain no more than one or two units constituted a response. The resting thresholds for these different responses ranged from 2 mA for the minimal response to 3 mA for a $\frac{1}{2}$ maximal response. The changes in threshold for ischaemia of different durations are shown in Fig. 4. After 10 min of ischaemia the threshold trajectories were not very different, especially when thresholds were plotted relative to their values at the end of ischaemia (Fig. 4*B*). After 15 min, however, the thresholds appeared to fall on one of two preferred trajectories. The highest threshold fibres followed an upper trajectory without a notch, and the lower threshold fibres a lower trajectory with a small notch. Trace 2, corresponding to a $\frac{1}{4}$ maximal CMAP, formed the most prominent notch by switching rapidly from the higher to the lower trajectory.

The rapid switching suggested by the behaviour of trace 2 in Fig. 4*B* was investigated further by the experiment in Fig. 5. The maximum rate of change of the

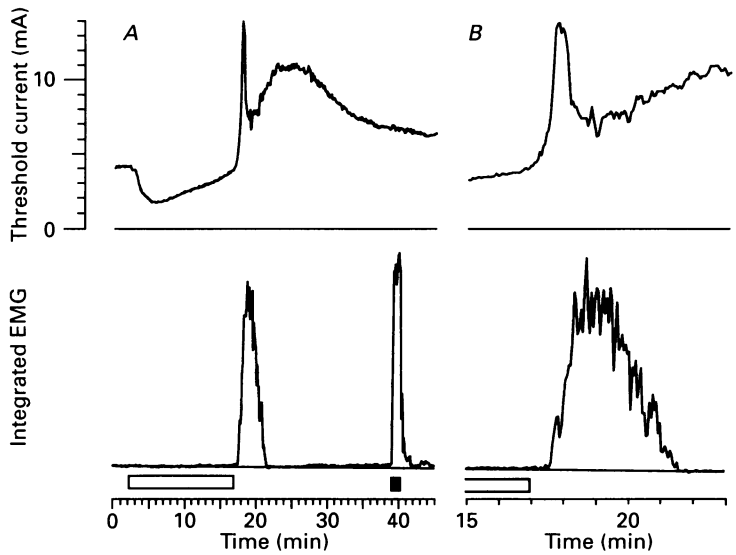

Fig. 3. Spontaneous activity and excitability changes after 15 min ischaemia. *A*, top, amplitude of 2 ms current pulses required to evoke $\frac{1}{5}$ maximal CMAP in ADM. Ulnar nerve stimulated under cuff above elbow. *A*, bottom, EMG integrated during intervals between stimuli to show spontaneous activity (not calibrated). Open bar, 15 min ischaemia. Filled bar, voluntary contraction to match integrated EMG. *B*, expansion of period from 15–23 min to show timing of spontaneous activity in relation to end of ischaemia and threshold changes.

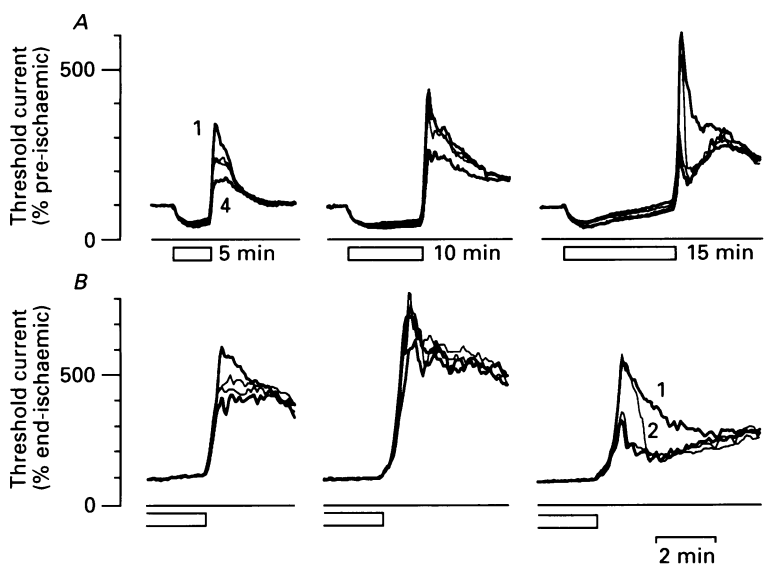

Fig. 4. Duration of ischaemia and homogeneity of excitability changes. Threshold changes to 5, 10, 15 min of ischaemia (open bars) obtained by tracking stimuli required to evoke CMAPs of different sizes. Traces 1–4 correspond to $\frac{1}{2}$, $\frac{1}{4}$, $\frac{1}{8}$ and $\frac{1}{40}$ maximal responses respectively. Traces 1 and 4 thick lines, 2 and 3 thin lines. *A*, threshold currents plotted relative to pre-ischaemic values. *B*, thresholds plotted on expanded time scale, relative to values just before deflating the pressure cuff.

stimulus was increased by tracking only two conditions ($\frac{1}{4}$ and $\frac{1}{8}$ maximal CMAP) and stimulating every 250 ms with a maximum step size of 9·4%. This allowed each stimulus to double in less than 4 s. This rate of stimulus increase was adequate to track the threshold increase after 5 min of ischaemia, which was similar for both sizes

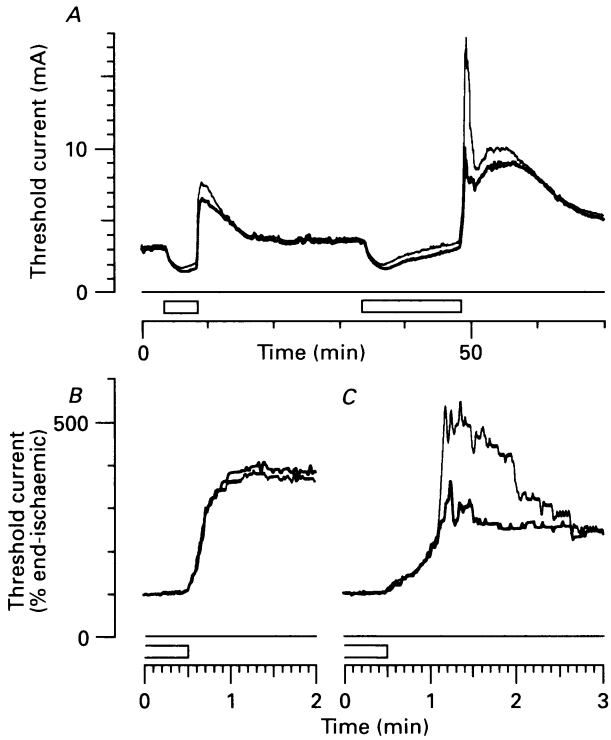

Fig. 5. Fast and slow excitability changes after prolonged ischaemia. *A*, threshold currents for $\frac{1}{4}$ maximal (thin trace) and $\frac{1}{8}$ maximal (thick trace) CMAPs in response to 5 and 15 min ischaemia (bars). *B*, threshold changes after 5 min ischaemia, replotted on expanded time scale and relative to values at end of ischaemia. *C*, thresholds after 15 min ischaemia plotted similarly, showing abrupt threshold increase for some fibres.

of CMAP (Fig. 5*B*). After 15 min of ischaemia, however, the threshold rise for a $\frac{1}{4}$ maximal CMAP fell into two distinct phases, a slow increase over 40 s followed by an abrupt rise that was too fast to track, a doubling in less than 4 s. The slow increase was followed almost exactly by the lower threshold fibres, but not the abrupt rise. The onset of the 'notch', which appeared another 40 s after the abrupt rise, involved a similarly rapid fall. This experiment confirmed our interpretation of Fig. 4, that a significant population of fibres could switch rapidly between two threshold states at times when there was most unlikely to be any abrupt change in their ionic environment or electrogenic pumping.

Experiments to test whether these abrupt changes were potential dependent are illustrated in Fig. 6. Thresholds were tested at the ends of 1 mA, 100 ms current ramps applied through the stimulating electrode. (The ramps were the first halves of 200 ms triangular current pulses.) Stimuli were delivered every 500 ms in the

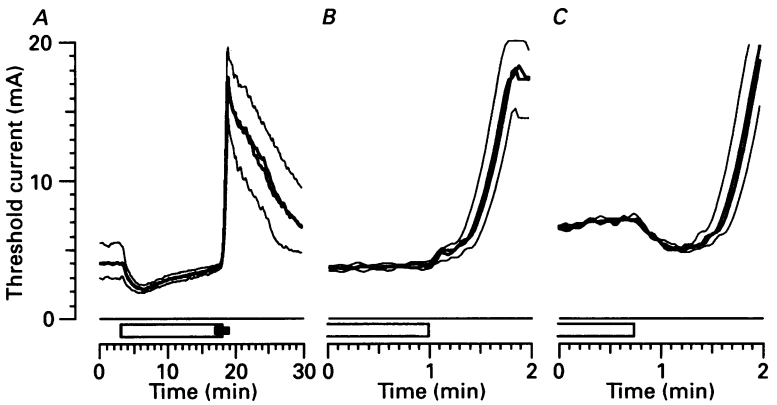

Fig. 6. Effect of polarizing currents on rapid threshold increase. Thresholds for $\frac{1}{4}$ maximal CMAPs recorded without polarizing current (thick traces) and with 1 mA hyperpolarizing and depolarizing currents (upper and lower thin traces respectively) applied through stimulating electrode (see text). *A*, open bar, 15 min ischaemia; filled bar indicates time of expanded record in *B*. *C*, similar detail of thresholds following 20 min ischaemia.

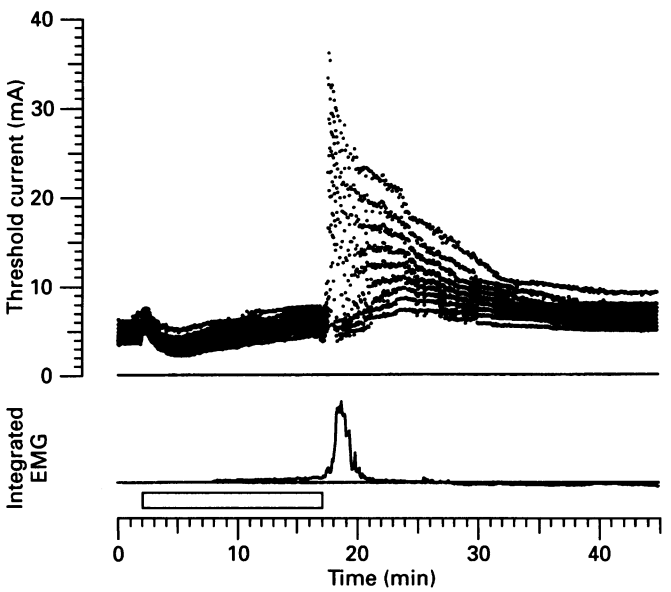

Fig. 7. Threshold distributions. Top, data from repeated stimulus–response determinations plotted as threshold distributions, each dot representing the threshold of fibres contributing 10% of the maximal CMAP (see Fig. 1). Bottom, integrated EMG recorded during intervals between stimuli to show time course of spontaneous activity (not calibrated). Open bar, 15 min ischaemia.

sequence: 1 ms control threshold test (thick trace), 1 ms test on 1 mA depolarizing current (lower thin trace), 1 ms control threshold test (thick trace), and 1 ms test pulse on 1 mA hyperpolarizing current (upper thin trace). In Fig. 6*A*, the separation of the thin traces provides a measure of the accommodation of the nerve to the 1 mA polarizing currents: during ischaemia the nerve accommodated strongly over

100 ms, and 1 mA produced a change in threshold much less than 1 mA, whereas during the post-ischaemia period there was 'negative accommodation' and a 1 mA polarizing current produced a change in threshold of several milliamps (see preceding paper). On an expanded time scale in Fig. 6*B*, the main effect of the polarizing currents was on the timing of the rapid phase of threshold rise. The stimulus started rising at its maximum rate (necessarily slower than in Fig. 5) about 11 s earlier with the 1 mA hyperpolarizing current than with the depolarizing current. A similar effect is shown in Fig. 6*C* after 20 min of ischaemia. These and two further recordings with polarizing currents showed that although they altered the timing of the rapid threshold rise, they had little if any effect on the level of threshold current (and therefore of membrane potential) at which it occurred.

The threshold trajectories in Fig. 4*B* suggested that there was a period after 15 min of ischaemia when the fibres were mostly to be found in one of two threshold states. To test this idea we recorded stimulus–response curves every few seconds, and derived threshold distributions as described in Methods. In the upper part of Fig. 7, each dot represents the threshold for fibres contributing 10% of the total CMAP. This shows that after cuff release the range of thresholds became much greater. The period between 15 and 25 min in Fig. 7 is expanded in Fig. 8, with thresholds plotted for every 5% of the CMAP, and on a logarithmic scale to show the distributions more clearly. A bimodal distribution of thresholds is evident for about 5 min after the usual abrupt threshold rise. Thresholds clustered about high and low values, which gradually converged.

The distributions over selected short periods are plotted more conventionally in Fig. 8*B*. In plot 1 of Fig. 8*B*, just after cuff release, the unimodal threshold distribution is similar to that during ischaemia. Plot 2, a minute later, shows a majority of fibres with high threshold, a few with low threshold, and a gap in between. The bimodality is not a consequence of impulse generation, since the spontaneous activity starts later. The bimodality is also not due to there being two constitutionally distinct populations of fibres, because there are fewer fibres in the high-threshold group in plot 4 than in plot 2. Some fibres have dropped down from a high threshold to low threshold, corresponding to the onset of the notch in Fig. 3. (The data in Figs 7 and 8 are entirely consistent with the data in Figs 3–5: a family of threshold trajectories like those in Fig. 4 may be constructed by joining together the dots in Fig. 7 corresponding to a particular fraction of the maximal CMAP.) Figure 8 therefore confirms our interpretation of the threshold trajectories, that single fibres can switch between low- and high-threshold states and back again. It also clarifies the behaviour of the two states. For example, the majority of fibres switch up to the high state and stay there, with threshold trajectories similar to those normally seen after 10 min ischaemia, and quite different from those exhibited by the more excitable fibres.

Figures 7 and 8 also show an interesting relationship between thresholds and spontaneous activity. Spontaneous activity was not generated simply when the threshold fell below a certain value, since thresholds were lowest during ischaemia when there was no motor activity. The spontaneous activity occurred after the post-ischaemic rapid rise in threshold, and when some fibres were in the high state and some in the low state. The activity was strongest between periods 2 and 3 in Fig. 8,

which was also the period when most of the dropping down from the high state to the low state occurred. This suggests that the spontaneous discharges may be triggered by discrete events, i.e. spontaneous transitions between the 2 states, rather than simply with a steady state of high excitability. This hypothesis is strongly supported by the model in the next section.

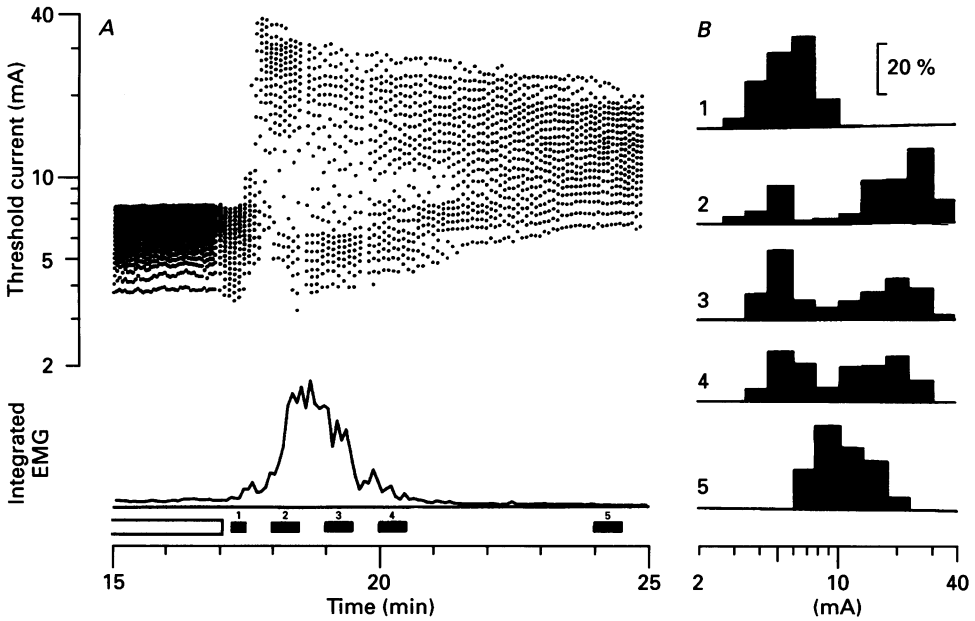

Fig. 8. Bimodal threshold distributions. *A*, expanded portion of Fig. 6, but with thresholds plotted on logarithmic scale and each dot representing fibres contributing 5% of the maximal CMAP. *B*, threshold distributions calculated directly from stimulus–response data (Fig. 1) for five periods indicated by numbered black bars at foot of *A*. The height of each bar represents the percentage contribution to the CMAP recruited by each 31·8% increase in stimulus. Note the increase in proportion of fibres in the low-threshold group from 18 to 20 min.

A model of human motor axons, during and after ischaemia

The model defined in Methods (Fig. 2) had a threshold for 1 ms current pulses (I_{th}) close to 0·4 nA (Fig. 10). Accommodation in the human nerve used for the excitability measurements is compared in Fig. 9 with electrotonus in the model for a range of stimulus currents set to the same fractions of I_{th}. For hyperpolarizing currents, electrotonus in the model provides a good match for the threshold electrotonus. For depolarizing currents there are significant differences, but these are not entirely due to inadequacies of the model. In part the multiunit nature of the nerve recordings may be responsible, since the responses of the model to $\pm 0{\cdot}4 \times I_{th}$ fit much better to the single-unit recordings of threshold electrotonus previously published by Bostock & Baker (1988). (The discrepancy between single-unit and multiunit recordings is suggestive of a local response in some fibres.) In part the differences reflect the fact that threshold is only an indirect measure of membrane potential. The accommodation revealed by threshold electrotonus in Fig. 9*A*

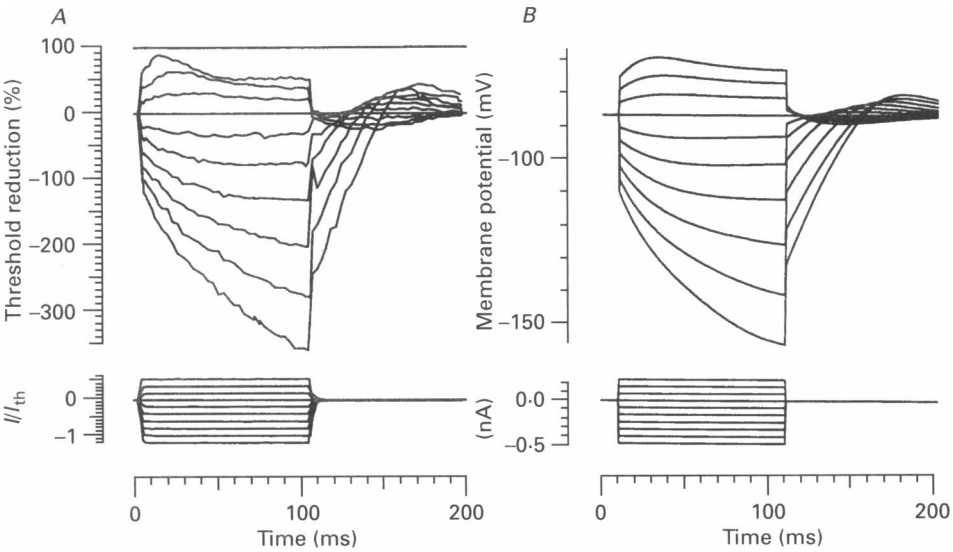

Fig. 9. Model of electrotonus in a human motor nerve. *A*, multiunit threshold electrotonus recorded from H.B.'s ulnar motor axons. *B*, electrotonus in mode, for currents corresponding to those in *A* (i.e. 0·6 to $-1{\cdot}2 \times I_{th}$, where I_{th}, the threshold for a 1 ms current pulse, was 0·4 nA).

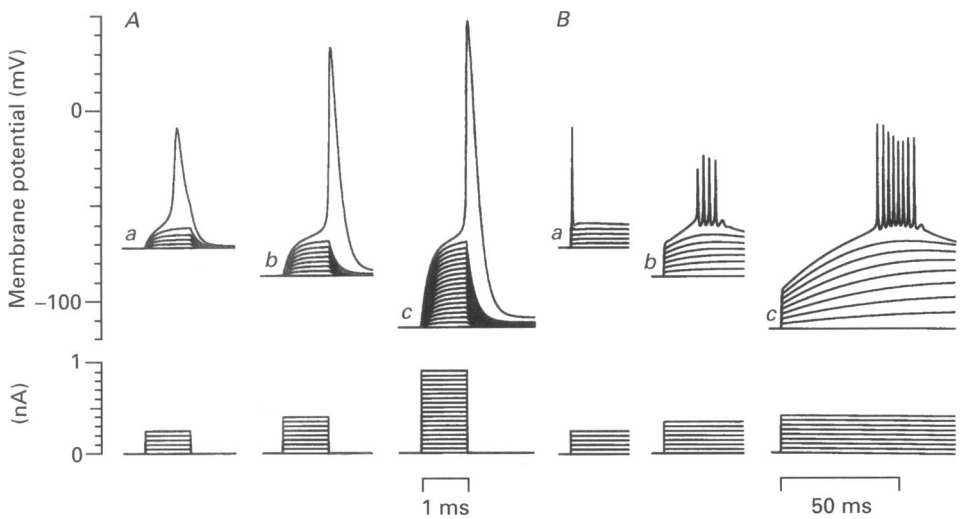

Fig. 10. Potential dependence of threshold behaviour of the model. Responses of the model to 1 ms (*A*) and rheobasic (*B*) current pulses increasing in 0·05 nA steps up to threshold: *b*, resting state (−86·7 mV); *a*, depolarized by blocking pump current and 9 mM $[K^+]_o$ (−71·9 mV); *c*, hyperpolarized by setting pump current to 0·6 nA (−114 mV). I_{rh} increases much less on hyperpolarization than I_{th}, and the latency to the first spike is prolonged.

includes accommodation due to a reduction in nodal resistance (e.g. because of activation of nodal K_s channels) as well as accommodation due to repolarization.

Some threshold behaviour of the model is illustrated in Fig. 10. This can be compared with the responses of human motor axons to moderate ischaemic depolarization and post-ischaemic hyperpolarization described in the preceding

paper (Fig. 5*A* and *B* in Bostock *et al.* 1991). The model accounts for several of the characteristics of human axons not predicted by classical models of myelinated nerve (e.g. Goldman & Albus, 1968): (1) at rest the rheobase ($I_{rh} \sim 0{\cdot}35$ nA) is significantly lower than the threshold to a 1 ms current pulse ($I_{th} \sim 0{\cdot}4$ nA), with a latency to the

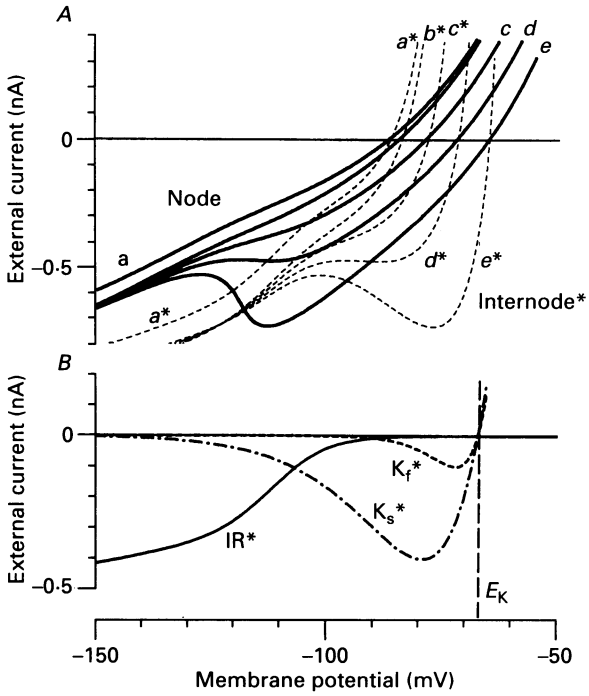

Fig. 11. Steady-state current–voltage relationships of model in simulated ischaemia. *A*: *I–V* curves for node (thick lines) and internode (* and thin, dashed lines); *a*, in normal resting state, $[K^+]_o = 3$ mM, *b–e* without pump current and progressive rundown of ionic gradients ($[K^+]_o = b$, 3 mM; *c*, 6 mM; *d*, 9 mM; e, 12 mM). *B*: some components of internodal current in 12 mM $[K^+]_o$, showing contribution of K_f and K_s channels to negative slope conductance. E_K is potassium equilibrium potential (−66·7 mV).

first spike (L_{rh}) 10–20 ms longer (Fig. 10*Ab* and *Bb*); (2) depolarization eliminates the difference between I_{th} and I_{rh} and reduces L_{rh} to L_{th} (Fig. 10*Aa* and *Ba*); (3) hyperpolarization increases I_{th} much more than I_{rh}, and also increases L_{rh} substantially (Fig. 10*Ac* and *Bc*); (4) similarly, hyperpolarization produces a prolonged (> 50 ms) phase of negative accommodation or continued depolarization to subthreshold current pulses (Fig. 10*Bc*); and (5) there is a small depolarizing after-potential (DAP) at rest, which is eliminated by depolarization and enhanced by hyperpolarization (Fig. 10*A*). A feature of normal human motor axons which appears exaggerated in Fig. 10*B* is their tendency to fire repetitively to a rheobasic stimulus. The model might be improved in this respect by inclusion of nodal K_f channels.

The steady-state current–voltage (*I–V*) relationship of the model is plotted in Fig. 11*Aa*, with the corresponding membrane potentials of the internode represented by the dashed line *a**. To simulate ischaemia, the pump current was first set to zero, but this only produced 2·2 mV of depolarization (Fig. 11*Ab*). Following inhibition of

the pump, the ionic gradients must run down, and this was simulated in Fig. 11*A c–e* by progressive equimolar reduction in $[K^+]_i$ and $[Na^+]_o$ and increase in $[K^+]_o$ and $[Na^+]_i$. The model depolarized, as expected, following the fall in potassium equilibrium potential E_K. An inflection and region of negative slope conductance

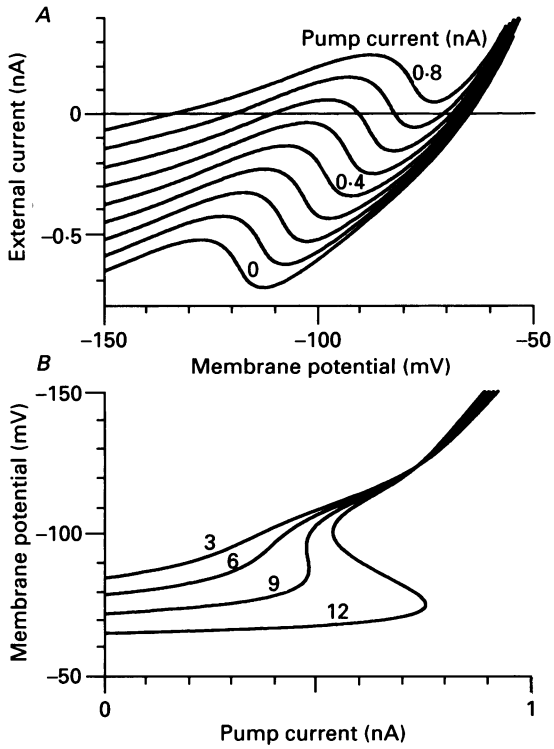

Fig. 12. Development of two stable states in simulated post-ischaemia. *A*, effects on nodal *I–V* in 12 mM $[K^+]_o$ (cf. Fig. 11*A e*) of increasing pump current. Node is depolarized for I_{pump} = 0–0·5 nA, hyperpolarized for $I_{pump} \geqslant 0{\cdot}8$ nA, and stable in both depolarized and hyperpolarized states for I_{pump} = 0·6, 0·7 nA. *B*, nodal membrane potential plotted as function of pump current for different values of $[K^+]_o$ indicated on lines (in mM). Model predicts two stable states and rapid phase of hyperpolarization for $[K^+]_o \geqslant 9$ mM.

appeared in the *I–V* curves when $[K^+]_o$ reached about 9 mM. The inflection only occurred at rather hyperpolarized potentials of the node, but close to the resting potential for the internode. Figure 11*B* shows that the negative slope conductance at 12 mM $[K^+]_o$ was mainly due to the internodal K_s channels.

To simulate the early post-ischaemic changes after $[K^+]_o$ had risen to 12 mM, the sodium pump current was increased in 0·1 nA steps (Fig. 12*A*). The inflection in the nodal *I–V* curve moved upwards and to progressively less negative membrane potentials, until at 0·6 nA there were two stable states of membrane potential (at −111 and −69 mV) and one state of unstable equilibrium. At 0·8 nA of pump current, there was only a single, hyperpolarized state, so that an axon behaving like the model would undergo an abrupt hyperpolarization by over 50 mV for a small increase in pump current.

To help relate this behaviour of the model to the post-ischaemic threshold changes

of human axons, the model data is replotted in Fig. 12*B*, with hyperpolarization as the ordinate and pump current as the abscissa. At low values of $[K^+]_o$, progressive activation of the pump produces a smooth hyperpolarization, but for $[K^+]_o$ greater than about 9 mM the model predicts an abrupt jump ('flip') from a depolarized up

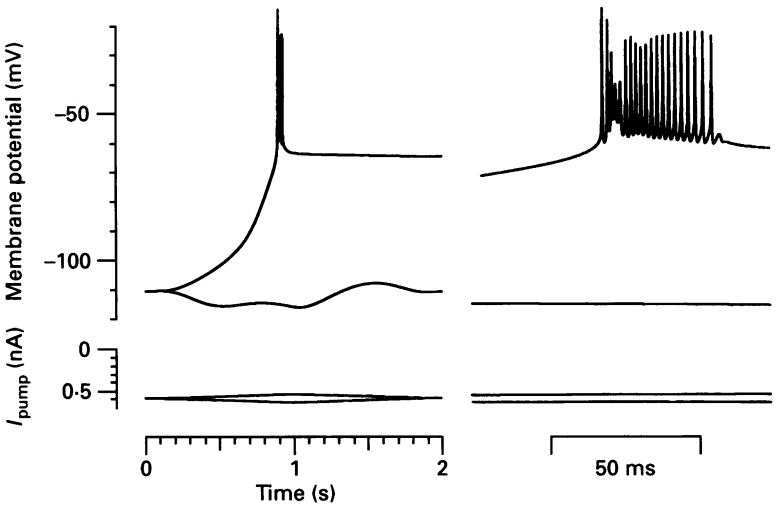

Fig. 13. Spontaneous burst discharge of model in high potassium. Time course of changes in membrane potential for small fluctuations of pump current for model in higher of two stable states, i.e. with 12 mM $[K^+]_o$ and 0·6 nA pump current. *A*, responses to slow 0·05 nA changes in pump current. *B*, expansion of period from 0·85 to 0·95 s in *A*.

to a hyperpolarized state. We propose that such 'flips' are responsible for the rapid phase of threshold rise recorded after long durations of ischaemia (see also Fig. 14 in the Discussion).

According to the threshold measurements in the first section, some fibres that have flipped to a high-threshold state subsequently drop down ('flop') to the low state. This could occur, according to the model, if there was a fall in pump current while $[K^+]_o$ remained high. The time course of such a transition from the high state to the low state is simulated in Fig. 13 for the case of 12 mM $[K^+]_o$. The high state with a pump current of 0·6 nA is rather unstable, and a small transient drop to 0·55 nA is sufficient to produce a large, irreversible depolarization. Although rapid compared with the time course of post-ischaemic pump activation, the depolarizing 'flop' is slow compared with an action potential, since it is limited by the rate of activation of K_s channels and the capacitance of the internodal axon. The most interesting point, as far as the origin of post-ischaemic motor fasciculations is concerned, is that the membrane potential temporarily overshoots the stable low potential resting state, producing a high frequency burst of action potentials (Fig. 13*B*). Two factors in the model were particularly important for this overshoot and the generation of action potentials: (a) activation of the IR channels in the high state, and (b) ultra-slow Na^+ channel inactivation, which reduced the steady-state excitability in the low state but was presumed to be removed during the period of hyperpolarization. The burst of action potentials was also dependent on the presence of Na^+ channels in the internode.

DISCUSSION

The most important new result reported in this paper is that post-ischaemic human motor axons can exist in two equilibrium states. The two states are distinguished by very different thresholds to brief current pulses, and therefore presumably very different membrane potentials. Suggestive evidence for the two states came firstly from the abrupt threshold rise that occurs after long periods of ischaemia, and is sometimes followed by an abrupt fall (e.g. Fig. 5). These large and rapid changes in excitability occurred when there was unlikely to be a correspondingly abrupt change in the environment of the fibres. Secondly, when excitability changes in different groups of fibres were followed by tracking the stimuli required to evoke different fractions of the maximal CMAP, they fell on one of two trajectories (e.g. Fig. 4*B*). The clearest evidence for the two states, however, came from the experiments in which we recorded threshold distributions repeatedly, and there was a period when the threshold distributions became bimodal (Fig. 8). In this discussion we will consider evidence from the model for the nature of the two states, and the hypothesis that the post-ischaemic ectopic discharges are caused by spontaneous 'flops' from the high state to the low state.

There have been no previous reports of myelinated axons existing in two stable states *in vivo*. Segal (1958) reported that squid giant axons in high potassium solutions exhibited threshold behaviour when hyperpolarized, switching between two stable states. Similar phenomena were observed in amphibian myelinated axons *in vitro* by Stämpfli (1959) and Tasaki (1959). The potassium concentrations used in those studies were generally greater than 20 mM, much higher than those required to block impulse conduction (10–15 mM). To help understand how two stable states could arise in human nerves at potassium concentrations insufficient block conduction, we turned to a model. Unfortunately no explicit models have been described that are appropriate for the human motor axons in having (a) membrane potential determined by ion concentrations and an electrogenic pump current, and (b) accommodation and excitability properties depending on membrane potential in the way described in the preceding paper (Bostock *et al.* 1991). The model presented here was intended to meet this need. It has obvious limitations, because it is based on only indirect and scanty information about the ion channels and pumps that determine membrane potential in human motor axons.

The equivalent circuit of Fig. 2 drastically simplifies the double cable structure of an internode, reducing paranodal and extended internodal axon membranes to a single element, as first done by Barrett & Barrett (1982). Internodes are now considered to have a non-uniform distribution of ion channels (Roper & Schwarz, 1989), and they may well deviate significantly from the assumed isopotential condition, especially during impulse activity. However, in the present state of knowledge a model with more elements and more unknowns would not be justified. We have also simplified the cable structure by representing a long length of axon by only a single node and internode. We have therefore not actually simulated impulse *conduction*. Nor have we represented the effects of spatial interactions during inhomogeneous repolarization, which some authors have suggested may be required for post-ischaemic impulse generation (Culp, Ochoa & Torebjörk, 1982; Bergmans,

1982*b*). Our results indicate that spatial gradients are not essential for this process, but an extended version of the model might have rather different dynamic behaviour.

The main justification for using a model that is bound to be in error in many quantitative details is that the most important conclusion we wish to draw from it is rather insensitive to the details. This conclusion is that the two stable threshold states of post-ischaemic nerve correspond to the two stable membrane potential states of the model, which arise because internodal K^+ channels (especially K_s channels) contribute a negative slope conductance to the I–V relationship in high $[K^+]_o$ (Fig. 11*B*). Over a limited potential range, hyperpolarized relative to E_K, depolarization increases the steady-state inward K^+ current by opening more channels. Internodal K_s channels have been shown to pass inward currents in high $[K^+]_o$ solutions by Grissmer (1986) in frog and Roper & Schwarz (1989) in rat. Any improvements in the assumed parameters for the K_s and other channels would not be expected to affect the propensity of the axons to exist in two stable states, though they might affect the particular value of $[K^+]_o$ at which a region of negative slope conductance for the whole axon first appeared.

The other element required to model the two post-ischaemic states was an electrogenic sodium pump capable of hyperpolarizing the axons by tens of millivolts. There is little direct evidence on the degree of electrogenic hyperpolarization in myelinated axons, but Lundberg & Oscarsson (1954) found that post-anoxic hyperpolarization of cat spinal roots could amount to 36% of the demarcation potential. Our localization of pump sites in the internode of the model may seem strange, in view of immunocytochemical evidence that Na^+–K^+-ATPase is restricted to nodal membrane (Ariyasu, Nichol & Ellismann, 1985). However, that study only demonstrated that the *density* of labelling was much higher at the nodes: the question of whether more Na^+–K^+-ATPase was present in nodes or internodes was left open. We have considered it likely that most electrogenic pumping is internodal because (a) 99·9% of the axolemma is internodal, (b) most of the resting sodium influx is internodal, (c) hyperpolarization by the pump, following short periods of ischaemia or trains of impulses, is not equivalent to applying hyperpolarizing currents. (For the same increase in I_{th}, the pump has a relatively greater effect in reducing accommodation and the threshold to ramp stimuli (Bostock *et al.* 1991) or in enhancing superexcitability (M. Baker, H. Bostock and P. Grafe, unpublished observations); these are all properties dependent on the resistance, and therefore the membrane potential of the internode. According to Fig. 2, a nodal pump current would be indistinguishable from externally applied current, hyperpolarizing the internode less than half as much as the node (Fig. 11*A*). In contrast, an internodal pump would hyperpolarize both almost equally, and therefore account for the discrepancies observed between the pump and external current sources.) If the pump sites were not mainly internodal, the model would still predict two stable states when the pump was activated in high $[K^+]_o$, but the states would occur at more hyperpolarized membrane potentials.

The second conclusion we would like to draw from the model, that bursts of impulses are generated by fibres spontaneously depolarizing from the high state to the low state, is more sensitive to the detailed assumptions, but supported by some

additional observations on human nerves. The depolarizing overshoot that followed a 100 ms hyperpolarizing current pulse applied to resting nerve (cf. Fig. 9) increased with increasing current strength, until the overshoot following a current of $-2\,I_{th}$ excited some fibres (in H.B.'s ulnar nerve). This did not occur immediately the

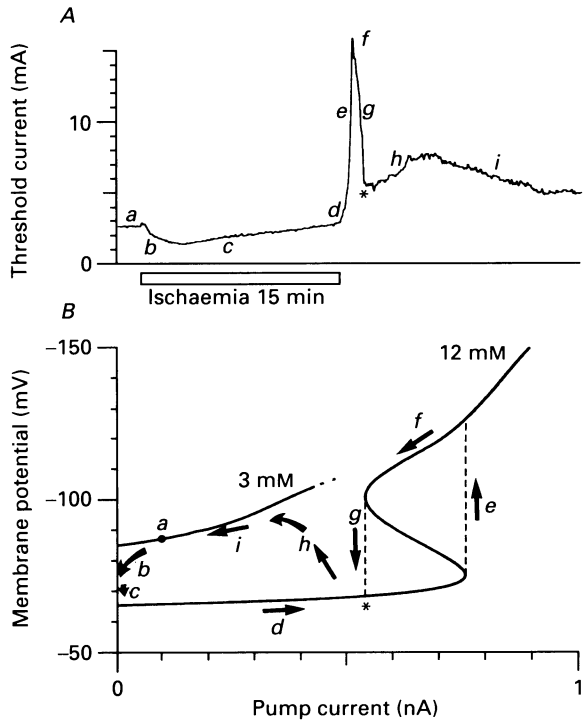

Fig. 14. Interpretation of ischaemic and post-ischaemic excitability changes in terms of changes in pump current and ionic gradients. *A*, changes in threshold for $\frac{1}{4}$ maximal CMAP and 15 min ischaemia (from Fig. 4, trace 2). *B*, dependence of membrane potential on pump current at 3 and 12 mM $[K^+]_o$ (from Fig. 12*B*). Small letters indicate suggested corresponding phases (see text).

hyperpolarizing current was terminated, like the anode break excitation of depolarized fibres (Baker & Bostock, 1989), but after a latency of 60 ms, corresponding to the peak of the threshold electrotonus (Fig. 9*A*). The model could not be excited by hyperpolarizing currents in this way, suggesting that human axons are actually *more* likely to be excited by a flop from hyperpolarized to depolarized state than the model.

Figure 14 summarizes our interpretation of the time course of excitability changes during and after ischaemia (*A*) in relation to the state diagram of the model (*B*). The resting state (*a*) is marked by the dot at 0·1 nA pump current in the curve for 3 mM $[K^+]_o$ (*B*). The first effect of ischaemia is to inhibit the resting pump current, but the consequent increase in $[K^+]_o$ also contributes to the early depolarization and drop in threshold (*b*) (Bergmans, 1979, 1982*b*). Further ischaemia produces a further rise in $[K^+]_o$ and more depolarization (*Bc*), but threshold slowly rises (*Ac*). This rise is not

due to the fibres being depolarized so far that further depolarization reduces excitability (Fig. 6*A*). Instead, it is probably due to a combination of ultra-slow sodium inactivation (Fox, 1976) and a fall in pH due to anaerobic glycolysis (Strupp, Bostock, Weigl, Piwernetz, Renner & Grafe, 1990). When circulation is restored, the sodium pump rapidly increases its activity (*Bd*), but because of the high $[K^+]_o$ this produces only a small repolarization (*Bd*) and slow rise in threshold (*Ad*), until the point of instability is reached. At this point the fibres flip (*e*) to the hyperpolarized, high threshold state. As the pump current subsequently slackens, the hyperpolarization and threshold are reduced (*f*) until the second point of instability is reached, and the fibres flop (*g*) back to the depolarized state, generating a burst of action potentials (*). $[K^+]_o$, affected by the circulation and Schwann cells as well as the axonal sodium pump, is restored more rapidly than $[Na^+]_i$: fibres in the low state therefore slowly hyperpolarize (*h*) due to the reduction in $[K^+]_o$ before the final recovery stage (*i*). Since some of the K^+ ions must be removed by the circulation, it is likely that an undershoot in $[K^+]_o$ contributes to this last phase (*i*) (cf. Bostock & Grafe, 1985).

The trajectory illustrated in Fig. 14 is only followed by a minority of fibres. For the least excitable ones (perhaps the smallest, with a greater rise in $[Na^+]_i$ and therefore relatively more pump activation) the high state is more stable, and a simpler path *a–b–c–d–e–f–i* is followed. An example is given by the upper row of dots in Fig. 7. For the most excitable fibres, perhaps the largest with relatively little pumping, the point of instability is not reached, and the path *a–b–c–d–h–i* is followed. The corresponding example is the lowest row of dots in Fig. 7. (Even the most excitable fibres seem to give a small, transitory rise in threshold, but this could be due to an ephaptic influence of the other, hyperpolarizing fibres, rather than a genuine change of state.) The lower path *a–b–c–d–h–i*, in which depolarization by $[K^+]_o$ counteracts hyperpolarization by the pump during the first 10 min after ischaemia, also provides an explanation for the behaviour of ulnar fibres innervating flexor carpi ulnaris (FCU), illustrated in Fig. 1*B* of the preceding paper (Bostock *et al.* 1991). A third and most important variant of the threshold trajectory illustrated is required to account for the observation first made by Kugelberg (1946) that the post-ischaemic discharges normally occur not in single bursts, as in Fig. 13, but in a series of bursts, repeated at intervals of about a second. Figure 14*B* suggests a possible mechanism for these repeated bursts. After the first flop (*g*) generates a burst of action potentials (*), the pump would be accelerated by the additional sodium influx, causing further hyperpolarization and a second flip. This cycle could repeat many times, giving an overall trajectory $a–b–c–d–(e–f–g–*)_n–e–f–g–h–i$.

In conclusion, human motor axons can exist in two stable states following ischaemia, and we suggest that the motor fasciculations are caused by spontaneous transitions from the high-threshold to the low-threshold state. It seems likely that this mechanism is also involved in other, related types of ectopic discharge, i.e. the post-ischaemic discharges in human sensory fibres responsible for paraesthesiae (Ochoa & Torebjörk, 1980), post-tetanic discharges following prolonged stimulation at 300 Hz in human motor axons (Bergmans, 1982*a*), and the corresponding phenomenon in human sensory fibres (Applegate & Burke, 1989). In each case a moderate insult produces hyperpolarization, as evidenced by enhanced super-

excitability and a rise in I_{th}, but after a prolonged insult axons fire ectopically, in high frequency bursts (Bergmans, 1982*b*). Our hypothesis reconciles the apparently contradictory proposals previously argued for these conditions, that the fibres must be hyperpolarized by the sodium pump (Bergmans, 1982*b*) and depolarized by extracellular potassium accumulation (Applegate & Burke, 1989). It remains to be seen whether our two-state model is applicable to any of the pathological conditions in which ectopic firing in axons has been implicated (Diamond, Ochoa & Culp, 1982).

This work was supported by the Medical Research Council. We would like to thank Professor T. A. Sears for comments on the manuscript.

REFERENCES

APPLEGATE, C. & BURKE, D. (1989). Changes in excitability of human cutaneous afferents following prolonged high-frequency stimulation. *Brain* **112**, 147–164.

ARIYASU, R. G., NICHOL, J. A. & ELLISMAN, M. H. (1985). Localization of sodium/potassium adenosine triphosphatase in multiple cell types of the murine nervous system with antibodies raised against the enzyme from kidney. *Journal of Neuroscience* **5**, 2581–2596.

BAKER, M. & BOSTOCK, H. (1989). Depolarization changes the mechanism of accommodation in rat and human motor axons. *Journal of Physiology* **411**, 546–561.

BAKER, M., BOSTOCK, H., GRAFE, P. & MARTIUS, P. (1987). Function and distribution of three types of rectifying channel in rat spinal root myelinated axons. *Journal of Physiology* **383**, 45–67.

BARRES, B. A., CHUN, L. Y. & COREY, D. P. (1988). Ion channel expression by white matter glia: I. Type 2 astrocytes and oligodendrocytes. *Glia* **1**, 10–30.

BARRETT, E. F. & BARRETT, J. N. (1982). Intracellular recordings from vertebrate myelinated axons: mechanism of the depolarizing afterpotential. *Journal of Physiology* **323**, 117–144.

BERGMANS, J. (1979). Electrogenic contribution to the normal membrane potential in single human nerve fibres. *Acta Neurologica Scandinavica* **60**, suppl. 73, 179.

BERGMANS, J. (1982*a*). Repetitive activity induced in single human motor axons: a model for pathological repetitive activity. In *Abnormal Nerves and Muscles as Impulse Generators*, ed. CULP, W. J. & OCHOA, J., pp. 393–418. Oxford University Press, New York.

BERGMANS, J. (1982*b*). Modifications induced by ischaemia in the recovery of human motor axons from activity. In *Abnormal Nerves and Muscles as Impulse Generators*, ed. CULP, W. J. & OCHOA, J., pp. 419–444. Oxford University Press, New York.

BOSTOCK, H. & BAKER, M. (1988). Evidence for two types of potassium channel in human motor axons *in vivo*. *Brain Research* **462**, 354–358.

BOSTOCK, H., BAKER, M., GRAFE, P. & REID, G. (1991). Changes in excitability and accommodation of human motor axons following brief periods of ischaemia. *Journal of Physiology* **441**, 513–535.

BOSTOCK, H. & GRAFE, P. (1985). Activity-dependent excitability changes in normal and demyelinated rat spinal root axons. *Journal of Physiology* **365**, 239–257.

CHIU, S. Y. & SCHWARZ, W. (1987). Sodium and potassium currents in acutely demyelinated internodes of rabbit sciatic nerve. *Journal of Physiology* **391**, 631–649.

CULP, W., OCHOA, J. & TOREBJÖRK, E. (1982). Ectopic impulse generation in myelinated sensory fibers in man. In *Abnormal Nerves and Muscles as Impulse Generators*, ed. CULP, W. J. & OCHOA, J., pp. 490–512. Oxford University Press, New York.

DIAMOND, J., OCHOA, J. & CULP, W. J. (1982). An introduction to abnormal nerves and muscles as impulse generators. In *Abnormal Nerves and Muscles as Impulse Generators*, ed. CULP, W. J. & OCHOA, J., pp. 3–26. Oxford University Press, New York.

DUBOIS, J. M. (1981). Evidence for the existence of three types of potassium channels in the frog Ranvier node membrane. *Journal of Physiology* **318**, 297–316.

FOX, J. M. (1976). Ultra-slow inactivation of the ionic currents through the membrane of myelinated nerve. *Biochimica et Biophysica Acta* **426**, 232–244.

GOLDMAN, L. & ALBUS, J. S. (1968). Computation of impulse conduction in myelinated fibres: theoretical basis of the velocity–diameter relation. *Biophysics Journal* **8**, 596–607.

GRISSMER, S. (1986). Properties of potassium and sodium channels in frog internode. *Journal of Physiology* **381**, 119–134.

HALLIWELL, J. V. & ADAMS, P. R. (1982). Voltage-clamp analysis of muscarinic excitation in hippocampal neurons. *Brain Research* **250**, 71–92.

KUGELBERG, E. (1946). 'Injury activity' and 'trigger zones' in human nerves. *Brain* **69**, 310–324.

KUGELBERG, E. & COBB, W. (1951). Repetitive discharges in human motor nerve fibres during the post-ischaemic state. *Journal of Neurology, Neurosurgery and Psychiatry* **14**, 88–94.

LEECH, C. A. & STANFIELD, P. R. (1981). Inward rectification in frog skeletal muscle fibres and its dependence on membrane potential and external potassium. *Journal of Physiology* **319**, 295–309.

LUNDBERG, A. & OSCARSSON, O. (1954). Anoxic depolarization of mammalian nerve fibres. *Acta Physiologica Scandinavica* **30**, suppl. 3, 99–100.

MAYER, M. L. & WESTBROOK, G. L. (1983). A voltage-clamp analysis of inward (anomalous) rectification in mouse spinal sensory ganglion neurones. *Journal of Physiology* **340**, 19–45.

MERRINGTON, W. R. & NATHAN, P. W. (1949). A study of post-ischaemic paraesthesiae. *Journal of Neurology, Neurosurgery, and Psychiatry* **12**, 1–18.

OCHOA, J. L. & TOREBJÖRK, H. E. (1980). Paraesthesiae from ectopic impulse generation in human sensory nerves. *Brain* **103**, 835–853.

ROPER, J. & SCHWARZ, J. R. (1989). Heterogeneous distribution of fast and slow potassium channels in myelinated rat fibres. *Journal of Physiology* **416**, 93–110.

SCHWARZ, J. R. & EIKHOF, G. (1987). Na currents and action potentials in rat myelinated nerve fibres at 20 and 37 °C. *Pflügers Archiv* **419**, 569–577.

SEGAL, J. R. (1958). An anodal threshold phenomenon in the squid giant axon. *Nature* **182**, 1370.

SHRAGER, P. (1989). Sodium channels in single demyelinated mammalian axons. *Brain Research* **483**, 149–154.

STÄMPFLI, R. (1959). Is the resting potential of Ranvier nodes a potassium potential? *Annals of the New York Academy of Sciences* **81**, 265–284.

STRUPP, M., BOSTOCK, H., WEIGL, P., PIWERNETZ, K., RENNER, R. & GRAFE, P. (1990). Is resistance to ischaemia of motor axons in diabetic subjects due to membrane depolarization? *Journal of the Neurological Sciences* **99**, 271–280.

TASAKI, I. (1959). Demonstration of two stable states of the nerve membrane in potassium rich media. *Journal of Physiology* **148**, 306–331.